ADVANCED SCIENCE
Open Access

Supporting Information

for *Adv. Sci.*, DOI: 10.1002/advs.201600504

Carbon Nanotubes in TiO_2 Nanofiber Photoelectrodes for High-Performance Perovskite Solar Cells

*Munkhbayar Batmunkh, Thomas J. Macdonald, Cameron J. Shearer, Munkhjargal Bat-Erdene, Yun Wang, Mark J. Biggs, Ivan P. Parkin, Thomas Nann, and Joseph G. Shapter**

((Supporting Information can be included here using this template))

Supporting Information

Carbon Nanotubes in TiO_2 Nanofiber Photoelectrodes for High Performance Perovskite Solar Cells

*Munkhbayar Batmunkh, Thomas J. Macdonald, Cameron J. Shearer, Munkhjargal Bat-Erdene, Yun Wang, Mark J. Biggs, Ivan P. Parkin, Thomas Nann, and Joseph G. Shapter **

Munkhbayar Batmunkh, Prof. Mark J. Biggs
School of Chemical Engineering,
The University of Adelaide,
Adelaide, South Australia 5005, Australia

Munkhbayar Batmunkh, Dr. Cameron J. Shearer, Munkhjargal Bat-Erdene, Prof. Joseph G. Shapter
School of Chemical and Physical Sciences,
Flinders University,
Bedford Park, Adelaide, South Australia 5042, Australia
E-mail: joe.shapter@flinders.edu.au

Dr. Thomas J. Macdonald, Prof. Ivan P. Parkin
Department of Chemistry,
University College London,
London, UK

Dr. Yun Wang
Centre for Clean Environment and Energy,
Griffith School of Environment, Gold Coast Campus, Griffith University,
Queensland 4222, Australia

Prof. Mark J. Biggs
School of Science,
Loughborough University,
Loughborough, Leicestershire, LE11 3TU, UK

Prof. Thomas Nann
MacDiarmid Institute for Advanced Materials and Nanotechnology,
School of Chemical and Physical Sciences, Victoria University of Wellington,
Wellington, New Zealand

Keywords: Photovoltaic, perovskite solar cells, photoelectrodes, TiO_2 nanofibers, carbon nanotubes

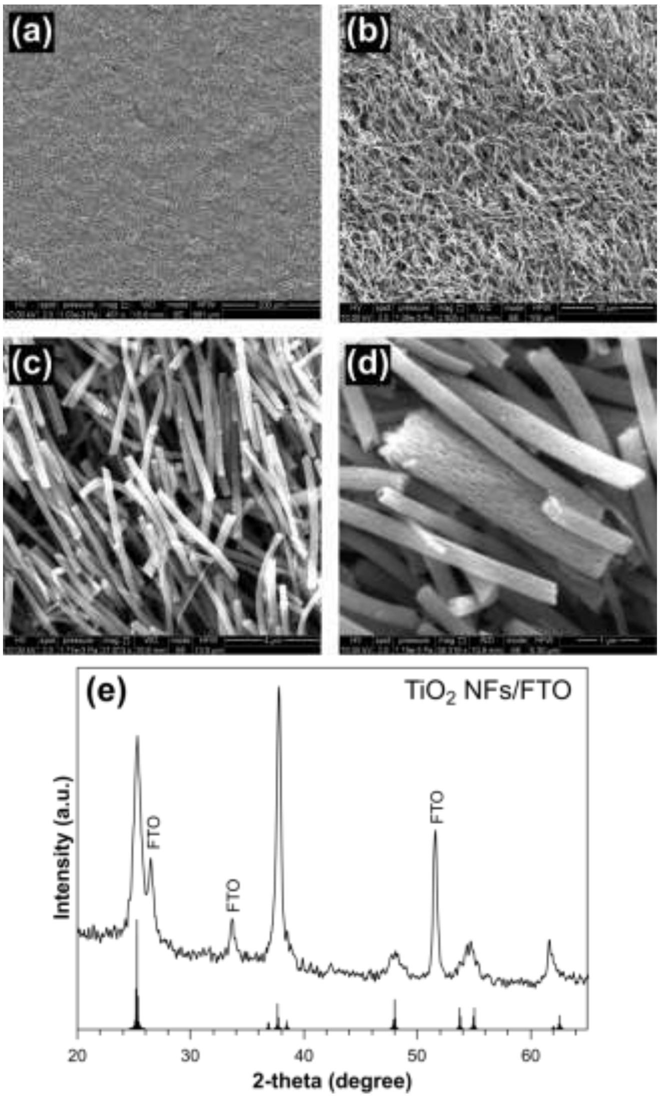

Figure S1. (a-d) SEM images of the electrospun TiO_2 NFs. (e) XRD pattern of TiO_2 NFs on FTO confirming the anatase phase with reference to 9853-ICSD.

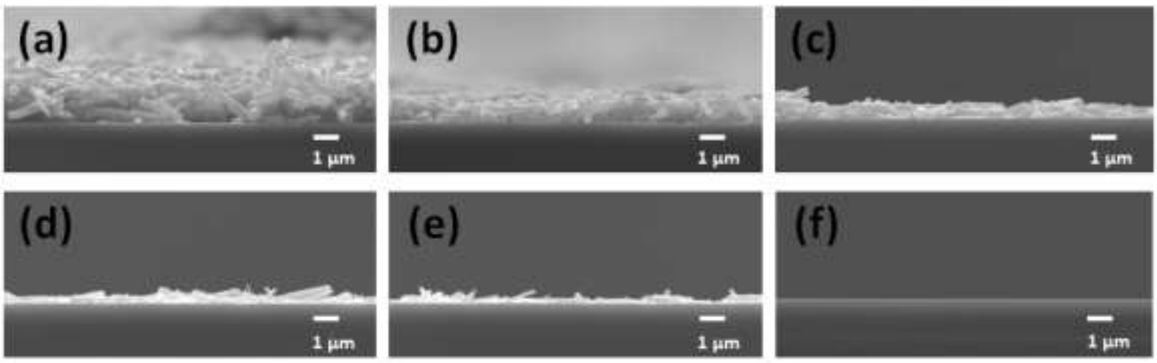

Figure S2. Cross sectional SEM images of TiO_2 NF photoelectrodes with the thickness of (a) ~2200 nm, (b) ~1300 nm, (c) ~580 nm, (d) ~400 nm, (e) ~285 nm and (f) 0 nm (planar).

Table S1. PV parameters of best performing PSCs fabricated with different TiO_2 NF thicknesses based photoelectrodes (extracted from the *J*–*V* characteristics reported in Figure 2a). The thicknesses of TiO_2 NF films for the fabrication of PSC devices are illustrated in Figure S2. The average PCEs of the cells were calculated based on at least five identical devices.

TiO_2 NFs thickness	J_{sc} (mA cm^{-2})	V_{oc} (V)	*FF*	PCE (%)	Average PCE (%)
2200 nm	11.58	0.75	0.58	5.01	4.77 ± 0.27
1300 nm	13.19	0.77	0.61	6.13	5.50 ± 0.47
580 nm	15.55	0.84	0.58	7.54	7.21 ± 0.36
400 nm	15.91	0.87	0.62	8.56	8.21 ± 0.46
285 nm	14.86	0.87	0.62	8.07	7.74 ± 0.44
0 nm (planar)	12.87	0.94	0.58	7.02	6.70 ± 0.44

Table S2. PV parameters of best performing PSC devices fabricated with different types of CNTs incorporated TiO_2 NF photoelectrodes (extracted from the *J*–*V* characteristics reported in Figure 2b). ~400 nm TiO_2 NF films were chosen for these cells. The concentration of CNTs in the TiO_2 NF-CNT hybrid was 0.02 wt%. The average PCEs of the cells were calculated based on at least five identical devices.

Device	J_{sc} (mA cm^{-2})	V_{oc} (V)	*FF*	PCE (%)	Average PCE (%)
TiO_2 NFs-only	15.91	0.87	0.62	8.56	8.21 ± 0.46
TiO_2 NFs-DWCNTs	16.71	0.88	0.62	9.04	8.81 ± 0.20
TiO_2 NFs-MWCNTs	17.07	0.86	0.62	9.08	8.97 ± 0.15
TiO_2 NFs-SWCNTs	17.20	0.93	0.62	9.91	9.69 ± 0.23

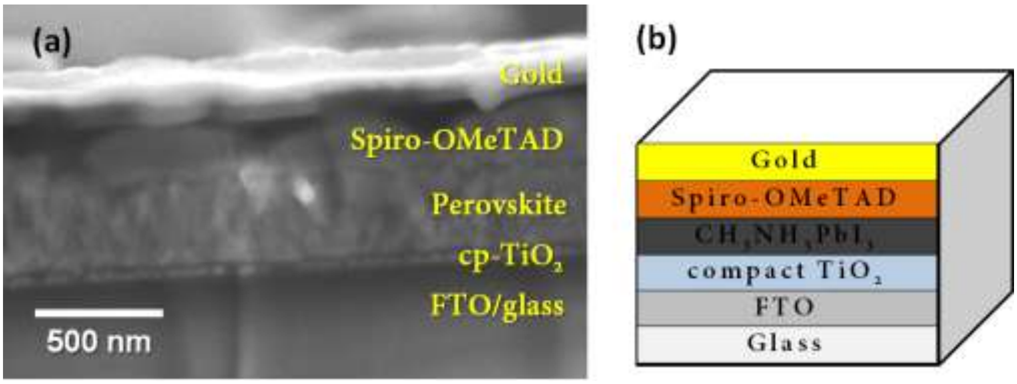

Figure S3. (a) Cross sectional SEM image and (b) schematic illustration of the planar PSC device structure.

The measurement of sheet resistance (R_s) of the TiO_2 NF-SWCNT thin films (on glass substrate) was carried out using a four point probe to investigate the mechanism of enhancement in the J_{sc} value of the devices. As shown in Figure S4, the R_s of TiO_2 NF films decreased gradually with increasing concentration of SWCNTs. This decrease in the R_s of the films is attributed to the high conductivity of SWCNTs that decreases the interfacial resistance between TiO_2 NFs.

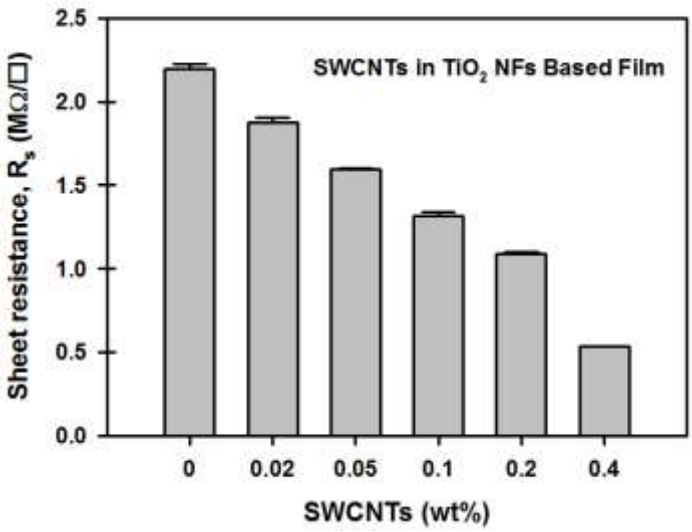

Figure S4. R_s of the TiO_2 NF films with various SWCNT loadings. Error bars are calculated from five different measurements.

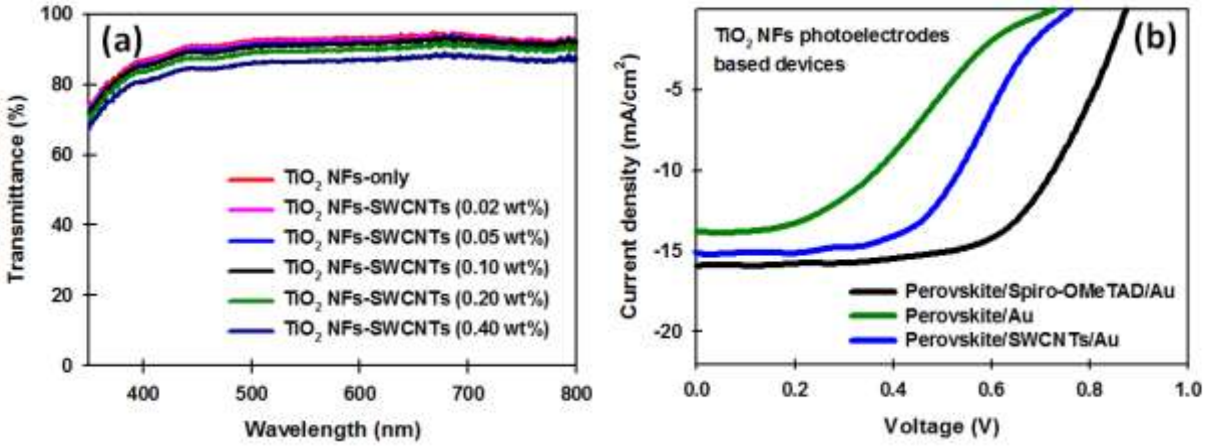

Figure S5. (a) Optical transmittance of the TiO_2 NF based films with different concentrations of SWCNTs. (b) *J–V* curves of TiO_2 NF-only photoelectrodes based PSCs with different hole transporting materials (HTMs).

Table S3. PV parameters of PSCs with and without SWCNTs in the photoelectrodes measured at forward and reverse *J–V* scans.

Device	Scan direction	J_{sc} (mA cm^{-2})	V_{oc} (V)	*FF*	PCE (%)
TiO_2 NFs-only	Forward	14.96	0.87	0.52	6.78
	Reverse	15.38	0.87	0.61	8.16
TiO_2 NFs-SWCNTs	Forward	18.76	0.92	0.57	9.86
	Reverse	18.89	0.93	0.64	11.44

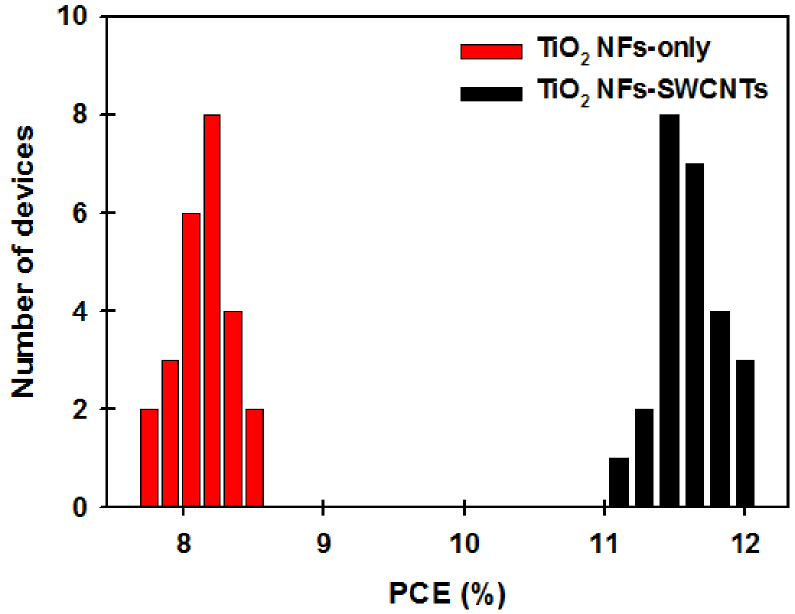

Figure S6. Histograms of PCE for the TiO_2 NFs-only and TiO_2 NF-SWCNT PSCs (measurement of 25 cells for each device structure).

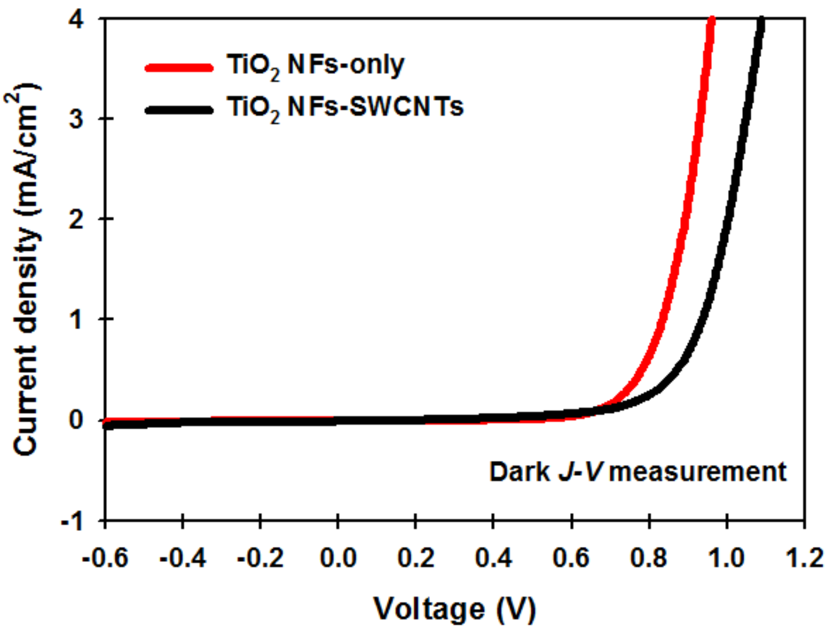

Figure S7. Dark *J-V* curves of PSCs fabricated based on TiO_2 NFs-only and TiO_2 NFs-SWCNTs photoelectrodes.

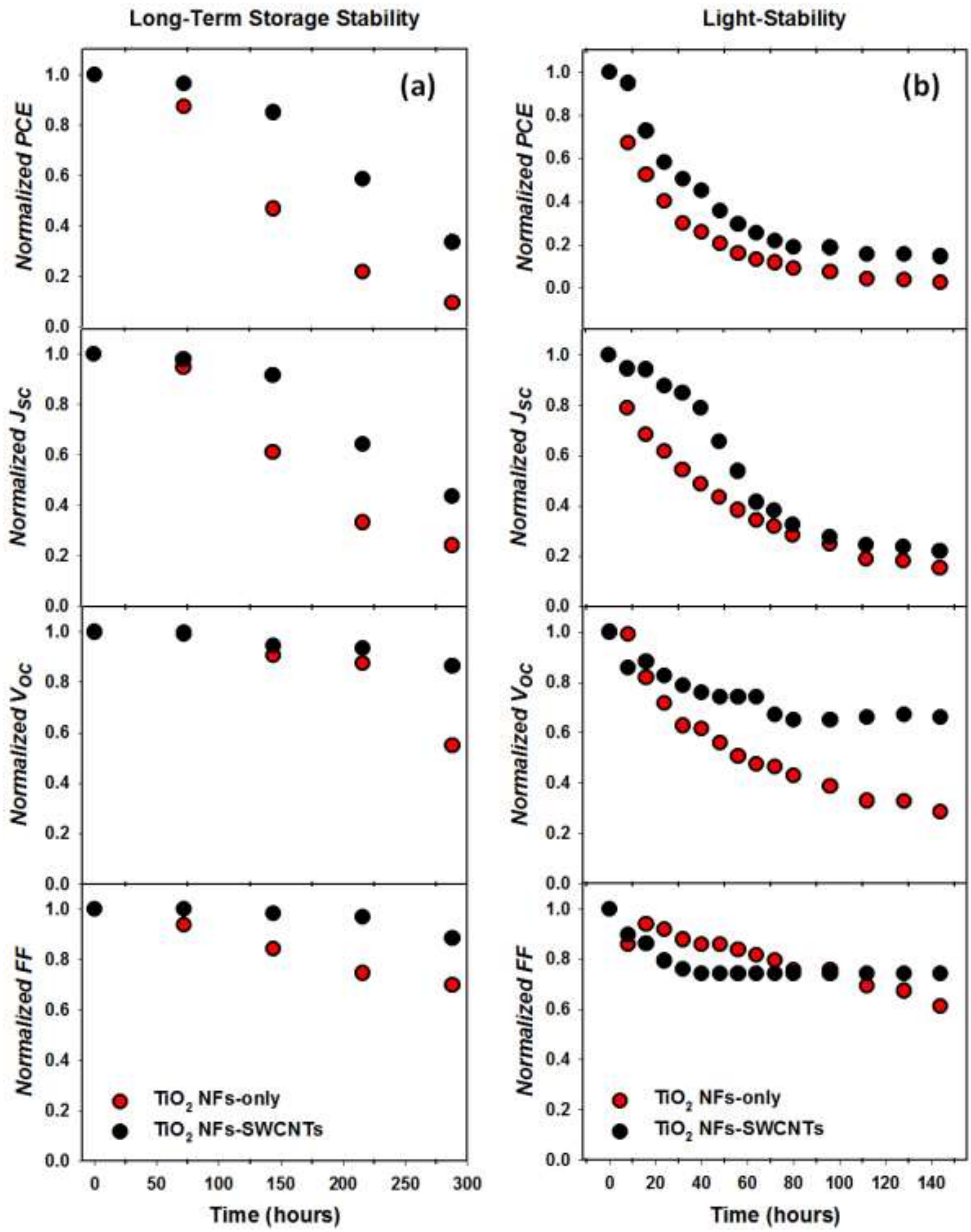

Figure S8. (a) Long-term storage- and (b) light-stability of the PSCs fabricated with and without SWCNTs in the TiO_2 NF photoelectrodes. For the long-term storage-stability, the fabricated cells were kept in the dark in ambient conditions for 288 h. The devices were not encapsulated for the stability test. For the light-stability test, the devices were exposed to continuous light illumination (100 mW cm^{-2}) in ambient conditions and the data were obtained in reverse scan direction at every 8 min. In Y-axis (normalized PV parameters), PCE(in), J_{sc}(in), V_{oc}(in) and FF(in) represents the initial (0 hr) PV values of the devices.

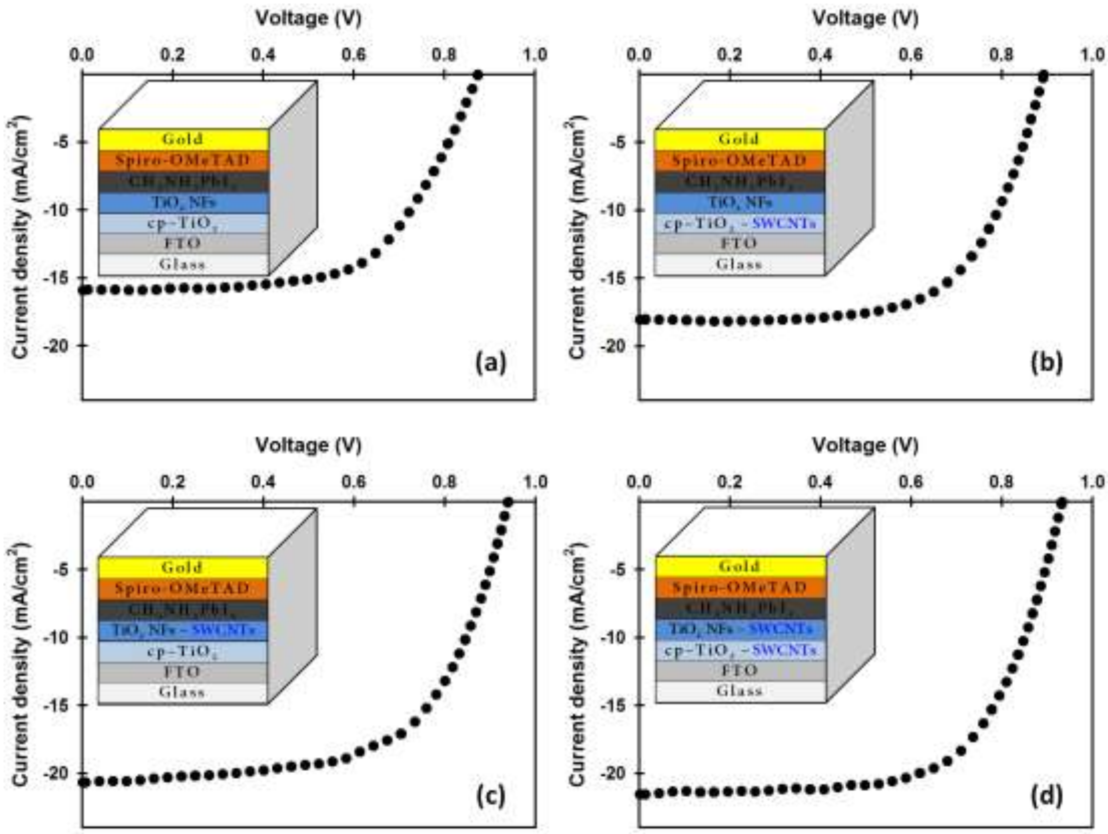

Figure S9. *J–V* curves of PSCs based on (a) compact (*cp*)-TiO_2 and TiO_2 NFs-only photoeletrode without any SWCNTs, (b) SWCNTs incorporated *cp*-TiO_2 layer and TiO_2 NFs-only photoelectrode, (c) *cp*-TiO_2 layer and SWCNTs incorporated TiO_2 NFs photoelectrode, and (d) SWCNTs incorporated into both *cp*-TiO_2 and TiO_2 NFs photoelectrode. An aperture mask was used during the *J–V* test.

Table S4. Detailed PV parameters of PSCs based on (Structure A) *cp*-TiO_2 and TiO_2 NFs-only photoeletrode without any SWCNTs, (Structure B) SWCNTs incorporated *cp*-TiO_2 layer and TiO_2 NFs-only photoelectrode, (Structure C) *cp*-TiO_2 layer and SWCNTs incorporated TiO_2 NFs photoelectrode, and (Structure D) SWCNTs incorporated into both *cp*-TiO_2 and TiO_2 NFs photoelectrode. The device structures are shown in the inset of Figure S9.

Device	J_{sc} (mA cm^{-2})	V_{oc} (V)	*FF*	PCE (%)	Average PCE (%)
Structure A	15.91	0.87	0.62	8.56	8.21 ± 0.46
Structure B	18.02	0.89	0.64	10.38	9.88 ± 0.43
Structure C	20.68	0.94	0.62	12.03	11.51 ± 0.40
Structure D	21.51	0.93	0.65	13.04	12.75 ± 0.43

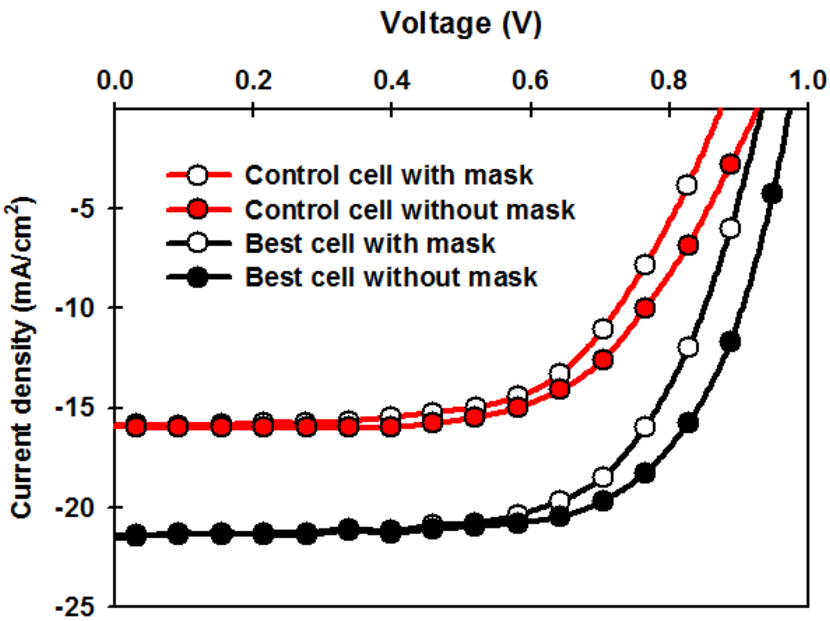

Figure S10. Effect of aperture masking on the *J–V* measurement of the PSC devices. The control cell is fabricated with the device structure shown in Figure 1a (without any SWCNT), while the best cell is made of structure such as that illustrated in the inset of Figure 9. The overlapped area of FTO electrode (anode) and gold electrode (cathode) was 0.14 cm^2. The aperture mask with an area of 0.081 cm^2 was used for the measurement with mask.